ATLAS Internal Note
TILECAL–NO–044
20–December–1994

Cell Intercalibration and Response Uniformity Studies Using a Movable Cs^{137} Source in the TILECAL 1994 Prototype

G. Blanchot, M. Bosman, M. Cavalli-Sforza, I. Efthymiopoulos,
Y. Ivanyushenkov, S. Orteu, J.A. Perlas, B. Ronceux, and F.Sanchez

Institut de Física d'Altes Energies, Universitat Autònoma de Barcelona

1 Introduction

The Tile Calorimeter design includes the possibility of running a radioactive source across axial holes in the rods compressing the calorimeter modules: this feature permits to check the response of each scintillator tile (fig.1). The current induced in the PMT is proportional to the gain of the PMT and to the photoelectron yield of the calorimeter for the scintillation light induced by the source.

Such a system was used to equalize the cell response of the calorimeter, and then to measure its uniformity and monitor changes in time. A first version of the system, using hardware developed at Notre Dame University, was used in 1993 to calibrate three prototype modules [1]: a thin flexible tube containing a Cs^{137} source was moved by a DC motor and its position measured by an encoder. The PMT current was measured by a pAmpmeter.

A second version was developed in 1994. Various aspects of the system were improved: increased speed of the source movement, uniformity of the steps, shorter readout time and implementation of on-line data analysis. With the new system, it was possible to intercalibrate the cells of the 5 calorimeter modules in a few hours and to perform various measurement during the runs taking

advantage of the beam-off periods. The hardware and data acquisition of the system developed in 1994 are described in this note, together with the results on calorimeter intercalibration and uniformity.

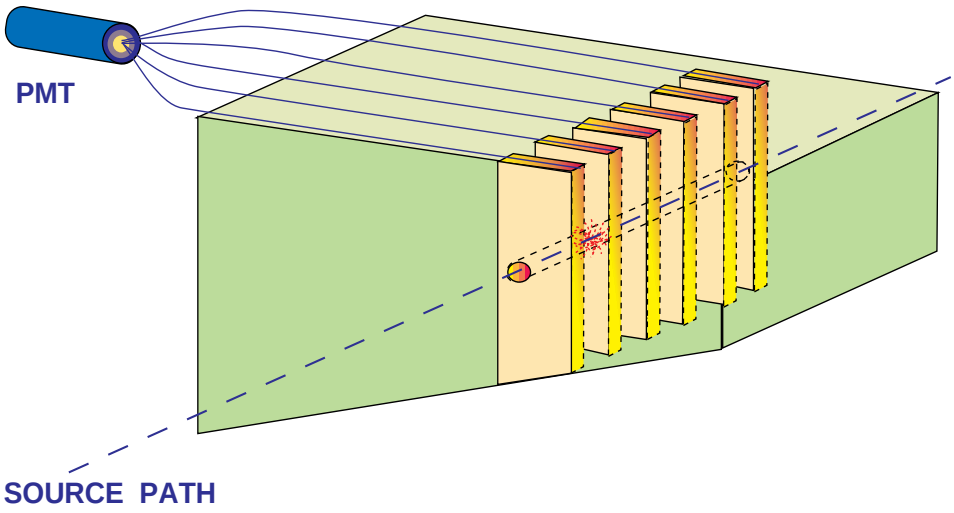

Figure 1: *Mechanical concept of the source calibration system*

2 Source scanner

A 5 mCi Cs^{137} source, 5 mm long, is embedded in a flexible stainless steel capillary tube (outer diameter of 0.7 mm) which can be inserted into the hollow rods across the calorimeter module. This tube is wound on a takeup reel of 15 cm diameter which is rotated by a stepping motor (M2) connected to the reel by a belt (Fig.2). The source end of the capillary tube is kept in a garage consisting of a cylinder of lead of 8 cm outer diameter. The takeup reel is coupled to a tone-arm mechanism, moving within a spiral groove on the bottom face of the reel. This mechanism trips a limit switch when the source is inside the garage, or when the source is maximally extended out of the reel.

The channel selecting mechanism consists of a carrier which slides on a rod and is driven by a threaded rod connected to another stepping motor (M1). The source tube is driven inside a flexible plastic tube, connecting the garage to the carrier, and is aligned by the carrier with one of the 100 holes in a fixed bar. These holes are in turn connected by plastic guiding tubes to the hollow rods of the calorimeter. Limit switches are provided to stop the carrier at the two ends and to count the holes as it is moved across the fixed bar.

To keep these tubes relatively short (1 to 3m), the source drive is placed on top of the calorimeter. Special care was taken to provide a smooth path to the source wire inside the tubes and across the connections. As a safety feature, when an obstacle in the unwinding of the tube from the reel is sensed, a limit switch stops the motor M2.

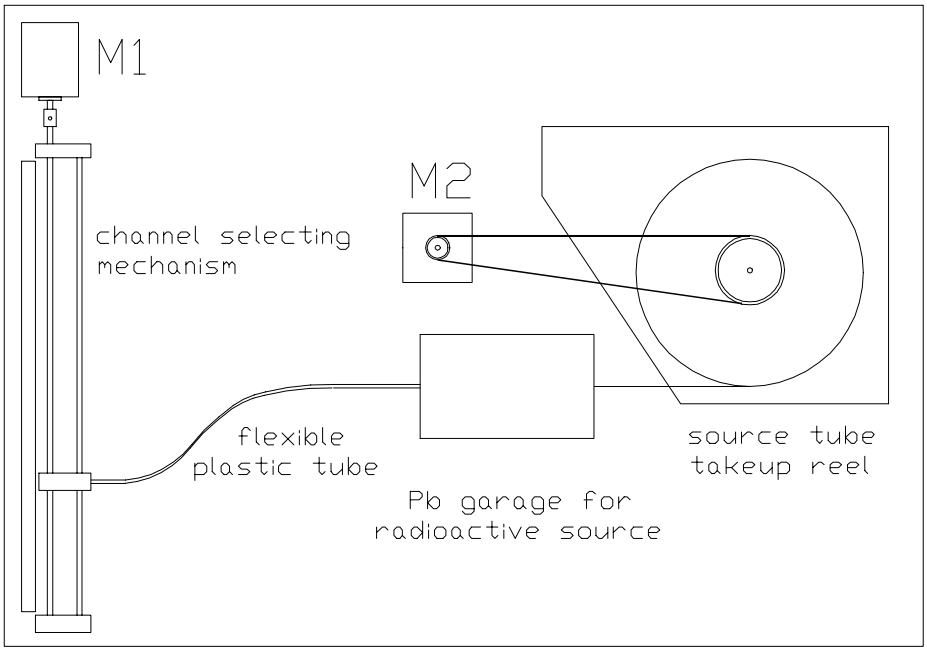

Figure 2: *Schematic diagram of the source moving machine*

3 Readout electronics

3.1 PMT signal

With the signals produced by the Cs^{137}, the PMTs may be regarded as current sources that produce current pulses of about 20 ns duration with a frequency of the order of 1 MHz. The amplitude of these pulses depends on the gain of the PMT: the expected mean current is about 300 nA which corresponds to pulses of 30 μA. The bases of the PMT (recovered from UA2) include a 10 kΩ resistance connected between the anode and the ground .

3.2 Current integrator

The purpose of the readout electronics is to measure the mean current of each PMT. This is achieved with an integrator circuit with a large time constant, set at 20 ms to filter the high frequencies of the signal, minimizing as well as possible the ripple on the DC output signal, but not larger to be able to see the slow variations of the current as the source moves across a cell. The DC output voltage is given by

$$V_{o-DC} = -R < i_{DC} >$$

where R is the feedback resistance and $< i_{DC} >$ the mean current to be measured (fig.3). The ripple ΔV due to the pulse structure of the signal is given by

$$\Delta V = \frac{i_{max}}{C}\tau$$

with C being the feedback capacitance and τ the pulse width; hence $\Delta V/V \simeq 10^{-4}$.

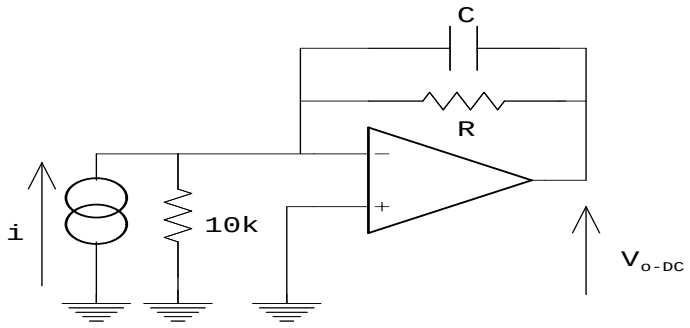

Figure 3: *Concept of the current integrator*

The DC output full scale is set at 5 V and the gain to 10^7 V/A . So the output voltage under nominal conditions is 3 V, which gives a comfortable dynamic range margin. Using a single stage integrator circuit this could be obtained with a feedback resistance of 10 MΩ. However in this case a single stage cannot be used because the offset voltage of the operational amplifier would be amplified in the following way:

$$A_{v_o} = \frac{R}{R_l} + 1$$

where R is the feedback resistance and R_l the PMT anode load resistance. This would result in an amplification of 1000 of the offset voltage and its potential drift, which is not acceptable. The solution to this problem (which is only due to

the presence of the anode load resistor) is to use amplifiers (OP27) with very low and stable offset voltage, and to divide the gain between two stages, each with an offset balancing network, for easier zeroing of the offset voltage (fig.4). The first circuit is the integrating circuit with a feedback resistance of 300 kΩ, the second being a single non inverting amplifier with a gain of 30. To achieve 20 ms time constant a feedback capacitance of 68 nF is used in the first stage.

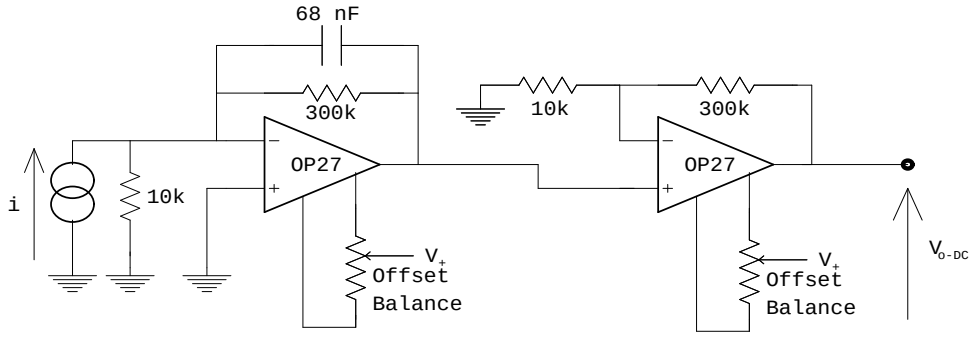

Figure 4: *Schematics of the current integrator*

3.3 Current integrator readout

A total of 200 integrator circuits were produced and installed in five NIM modules, each one reading 40 photomultiplier tubes (fig.5). The NIM modules are selected with a 3 bits address using single CMOS address decoders, and the 40 channels of each module are multiplexed (with a 6 bits address that controls a CMOS analog multiplexer matrix) to the input of a 12 bits ADC (AD7572AJN10) for digital conversion. For a 5 V full scale, the corresponding LSB is about 1.22 mV. The ripple of the DC signal, 300 μV is not seen by the ADC.

4 Data acquisition

4.1 Description of the system

In the design of the DAQ system for the calibration, two basic options were considered. The first one was to integrate it in the general DAQ system used for the test beam, as one of its special tasks. The second one was to develop a standalone system separated from the test beam DAQ. The first option presented

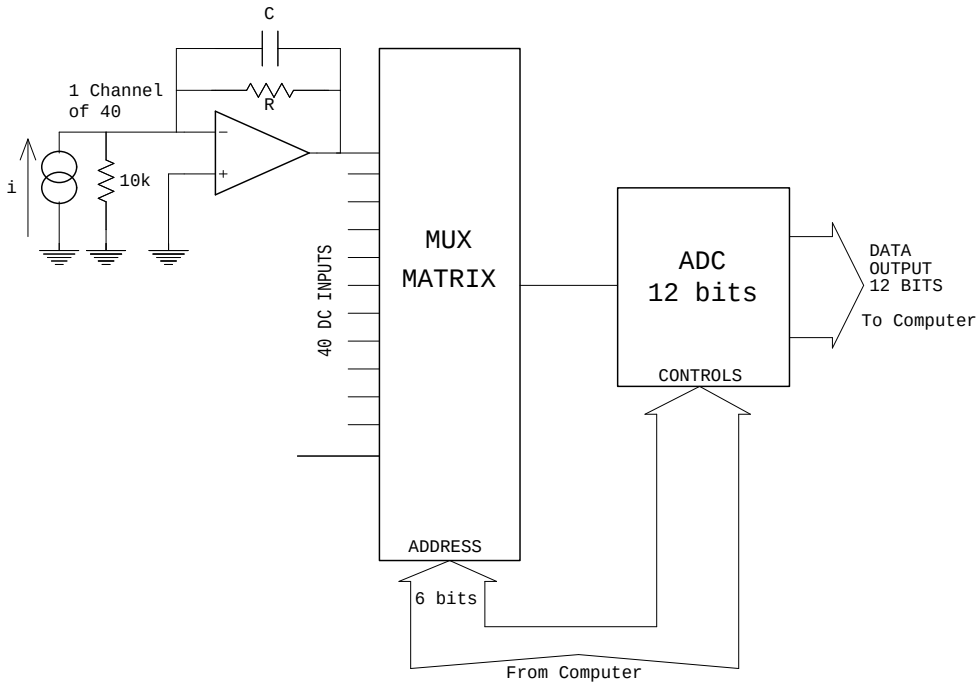

Figure 5: *Readout electronics for 40 PMTs (one NIM module)*

the advantage of a single DAQ environment, with the same electronics being used for calibration and normal DAQ. However, for reasons of portability and availability, important in the context of a test beam, the second option was selected.

The system was designed to achieve the following requirements:

- to fully control the movement of the wire carrying the Cs^{137} source, including security checks in case of mechanical failure,
- to control the readout electronics, optimizing the speed,
- to be powerful enough to analyze the data online, thus providing the fast feedback needed for the calibration procedure.

The basic component of the DAQ system is an IBM/PC-AT compatible computer. The DAQ software was developed using the National Instruments LabView package, a commercial software development package for instrument control, providing data acquisition and analysis as well as a graphics interface for data presentation. To control the external devices (motors and limit switches for the source moving machine) and the ADC readout from the current integrator electronics,

only digital electronics signals are needed (digital I/O and pulse generation and or counting). Plug-in Data Acquisition boards from National Instruments are suitable for such a task. This choice presents the additionnal advantage of making the integration of the software and hardware straightforward. In the following sections a detailed description of this system will be given.

4.1.1 Machine Control

Each of the two motors (hole selector and source driver) needs two digital signals, one to pulse the motor and one to control its direction. In addition, the various limit switches have to be monitored. These switches act as hardware stops in case the source would get out of control due to a hardware error, ensuring the safety of the system. They serve as well as reference for the initialization of the control procedure. These signals are sent or received by a DAQ plug-in board (PC-TIO-10) of National Instruments that includes 10 digital pulsers/counters and 16 digital I/O lines.

The software that controls the hole selector motor allows to move the source carrier to any selected hole. The system counts also the pulses generated by a switch every time the carrier passes in front of a hole. In case of discrepancy, the carrier is moved back to the starting position (hole 1). The system runs at 700 Hz which corresponds to about 6 min to move from hole 1 to hole 100. The motor that moves the source is controlled at a frequency of 200 Hz.

4.1.2 Current Integration DAQ

The readout of the current integrator electronics is done in two steps: the corresponding channel has to be selected by giving its address to the multiplexer and then the ADC is read. For these operations, only digital signals need to be exchanged. This task is performed by a plug-in data acquisition board PC-DIO-96 made by National Instruments, which provides a total of 96 digital I/O lines.

To address each of the 40 PMTs of a detector module (corresponding to one multiplexer channel) a total of 6 digital lines are needed. For the readout of an ADC, 12 data lines are needed as well as 3 digital signals to synchronize data conversion and readout.

4.1.3 User Interface

In the Cs calibration system, two LabView Virtual Instruments (VI) that perform specific task were created:

1. Move the source carrier from one hole to another: the input parameters to the VI are the current hole number and the target hole. The VI will start the motor and move the carrier to the desired position.

2. Acquire data from the 10 PMTs that correspond to a specific hole number: the input parameter of the VI is the hole number. The VI selects the 10 associated PMTs and measures their pedestals. It activates the motor controlling the wire, and pushes it inside the hole untill it reaches the end. The corresponding limit switch triggers. The motor starts then pulling the wire, stopping every 2.8 mm to measure the current. The data are displayed graphically, to have a visual control of their quality. At the end, the data are analysed (see section 4.3 for a description of the algorithm) and the result is displayed. Finally, all the information is saved in a file and archived on disk for offline processing.

4.2 Operation of the Cs source system

The time needed to move the source from the garage to the end of a tube is 70 s in case of the shortest tube. The time needed to scan a hole and make the about 430 current measurements is 155 s, to which one has to add 45 s to move the source back to the garage. So, the total time for a hole measurement is of the order of 5 min. The time per step is 360 ms. The largest contribution to that interval of time is not the mechanical movement (60 ms), nor the ADC conversion time (12 μs) but rather the handshaking with the computer in the conversion period. This is not an intrinsic limitation and could be substantially improved if the process were optimized. Typically, a full scan of a module (18 holes) was done in two hours.

4.3 Online data analysis

A typical spectrum of the current measured as the source moves across five cells is shown in Fig.6 for five of the PMTs that read those cells.

Five excitation curves, corresponding to the 5 readout cells, are superposed. Each curve presents a multiple peak/valley structure : the peak corresponds to the passage of the source across an individual scintillator (see section 7 for more details). The integral of the current spectrum, after baseline subtraction, provides a constant proportional to the gain of the corresponding PMT that can be used to intercalibrate the cells.

The integral of the current in a cell is evaluated with the following algorithm: one locates the position of the source where the maximum current was measured. Then, i_{max} is defined as the average current in a zone of $\pm 2.5cm$ centered on that point (a cell is 10 cm wide). The two edges of a cell are located by calculating the points where the current is 5% of i_{max}. The baseline is then estimated by averaging the currents in two reference zones, 2.5 cm wide situated at 12 cm respectively left and right from the cell edges, in order to take into account possible small drift of the pedestals after their measurement (done when the source was still in the garage). The final integral is obtained by summing the

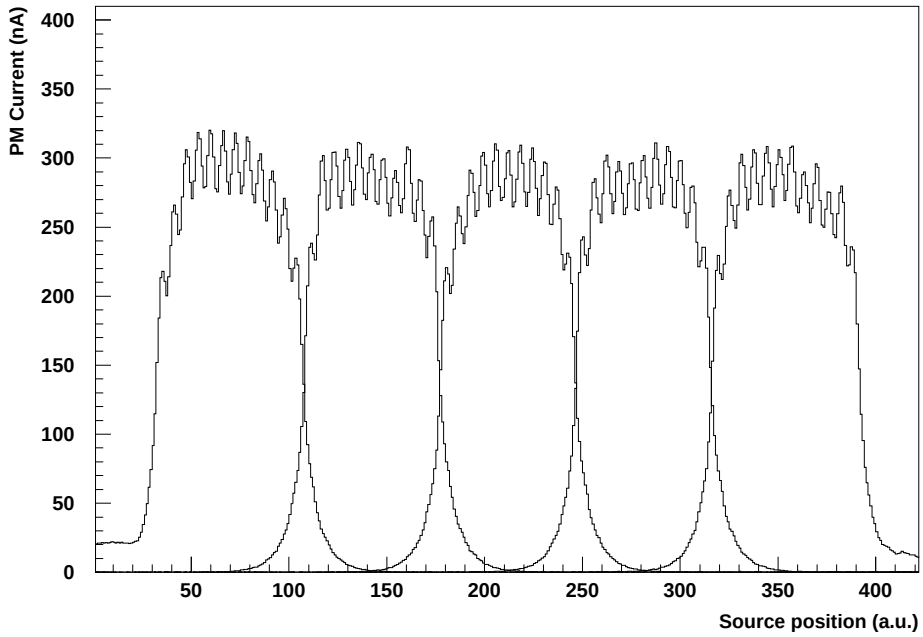

Figure 6: *Current measurement after pedestal substraction for the five PMTs on one tile side as a function of the source position*

measured currents in between the 2 outer reference zones and subtracting the average baseline.

The four PMTs situated at the edge of the calorimeter need a special treatment because for these cells the current spectrum is not symmetric. The reason is that a signal is induced by the source before it enters the calorimeter. For the rightmost (leftmost) PMTs only the left (right) baseline is computed. Then, the right (left) part of the curve that has a current smaller than 20% of the maximum is symmetrized to the left (right) part. Finally the integral is computed as before but using the new curve.

5 Calibration of the calorimeter

5.1 Gain setting procedure and calibration

The prototype calorimeter is composed of five modules segmented longitudinally in 4 samplings. The 4 samplings contain 3,4,5 and 6 tiles respectively. Each sampling is divided laterally in 5 cells, each cell being readout by 2 PMTs.

The first step of the calibration of the calorimeter is the adjustment of the gains of the 200 phototubes. The second tile in each sampling is scanned with the Cs source system providing the integral of the current measured by the 10

corresponding PMTs. All the values are adjusted using the known relation between the high voltage and the gain of every PMT. The scan is repeated until a good uniformity is achieved. This procedure allowed to adjust the integrals of the current measured in the 200 PMTs to better than 2% in 2-3 iterations typically.

The second step of the calibration consists in scanning all 18 tiles of a module[1]. The calibration constant for a PMT is given by averaging the measurements of all tiles in a given sampling, except the last one (see section 7 for further discussion).

5.2 Systematics and repeatability of the measurement

The method used to evaluate the integral of the current measured in a cell was described in section 4.3. The same method is used in the offline analysis. Systematic effects in the evaluation of the integral have been studied.

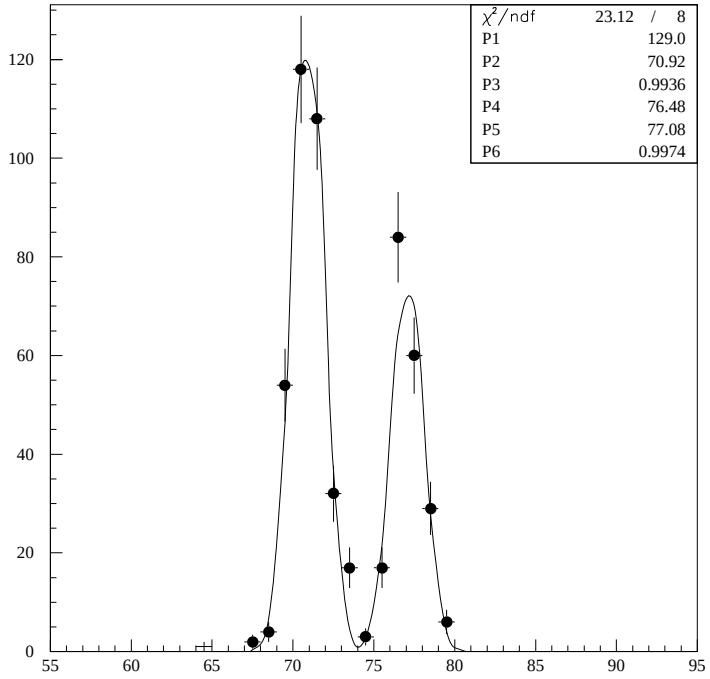

Figure 7: *Distribution of the FWHM in unit of measurement steps. two peaks are observed corresponding to the 2 different cell sizes : 11 and 12 periods respectively. The result of a double gaussian fit is shown on the figure (2 sets of parameters : p2(p5) is the mean , p3(p6) is the sigma, p1(p4) the normalization factor).*

The integral of the current measured in a cell is obtained by summing the individual measurements along a scan, assuming that the step is constant. Fig.7

[1]for the '94 test beam, the source scanner was connected to all 18 tiles of the central module and only 9 tiles for the other modules

shows the width of the cells measured during the scans: i.e. the FWHM of an excitation curve in number of steps. Two clear peaks are observed corresponding to the 2 cell sizes present in the calorimeter : the 3 central cells are composed of 11 periods of Iron/Scintillator Tiles (width = 19.8 cm), while the 2 outer cells are composed of 12 periods (width = 21.6 cm). From these distributions, one can infer that the step size was 2.8 mm . The 2 peaks have been fitted by a gaussian and give a sigma of 1 step. If that width would be fully attributed to fluctuation in the step size, it would correspond to a stability of the step of 1.4 %, which would translate in turn in a precision of the integral of 1.4 %. However, this is only an upper limit since at least two other factors contribute to the width of that distribution: the least-count error (± 0.4 steps), and the error on determining the FWHM from the response of a tile with the largest signal (fig.6).

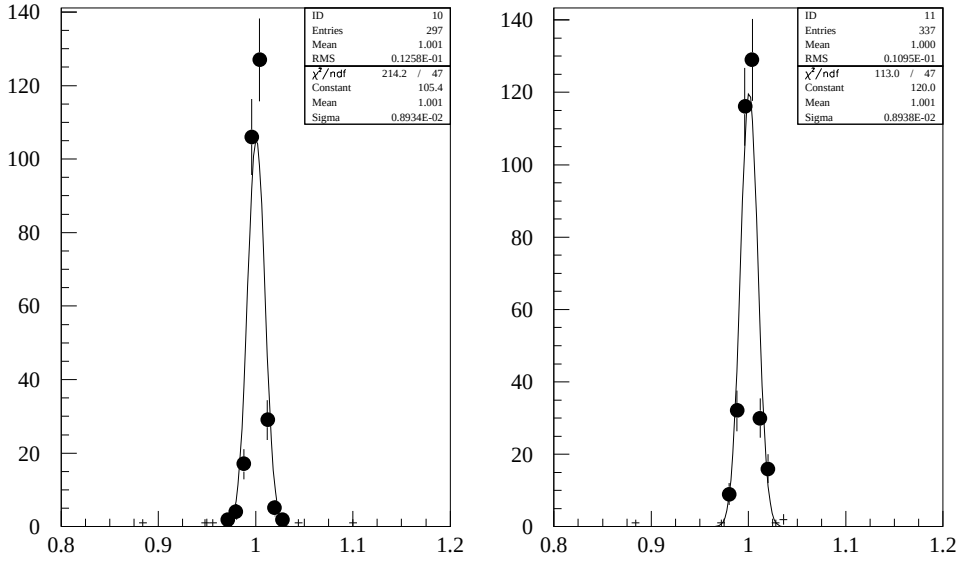

Figure 8: *Distribution of double ratios of calibration constants for August data (left) and September data (right) (see text). The sigma of those distributions is 0.9 % showing that the precision of an individual measurement is 0.5 %*

Different algorithms to evaluate the integral have been tested. The integrals obtained by summing the measurement in between the two FWHM points or by summing over the complete range agree to better than 0.8%. In order to estimate fluctuations due to the baseline subtraction, the baseline was computed over different ranges. The resulting integrals vary by less than 0.2%.

The repeatability of the measurements obtained with the Cs source was studied. The ratio of the integral measured for 2 rows of tiles readout by the same PMT is formed. In this ratio the gain of the PMT cancels; however it may be affected by systematic effects like different light yield for different tile sizes, dif-

ferent fiber lengths, etc. This same ratio is measured at a different time. Forming ratios of ratios, tile and fiber effects will cancel out. Fig.8 shows these double ratios for the August and September run: the sigma is 0.9%. Four measurements contribute to these double ratios, hence the precision of a single measurement is $0.9\%/\sqrt{4}$ or 0.5%, a factor two better than what was obtained in '93 [1]. This result shows as well that the step size is stable and is not the main effect contributing to the precision of the FHWM of a cell.

In conclusion, the study of possible systematic effects in the evaluation of the integral and of the repeatibility of the measurement, shows that the intrinsic precision of that integral is better than 1%.

6 Stability of the calorimeter calibration

The Cs source system was also used for the long-term monitoring of the calibration of the calorimeter. During the two '94 test beam periods, several partial or complete calibration scans were performed before and after the runs and during the 8 hours shutdown periods of the SPS. The distributions of ratios of gains measured at different time for the different modules are gaussian with a sigma of the order of 1-1.5 %, except for module 3 in august (3 %). In that case the gain of about one third of the PMTs varied by more than 5 %.

Fig.9 shows typical time evolution of the signals measured with the Cs movable source for 3 PMTs of the central module. They are shown as a function of the date: the August run took place from the 12th to the 24th of August and the September run from the 22th of September to the 12th of October. PMT 1 and PMT 9 on the figure are typical stable PMTs. PMT 3, which was unstable in August, was exchanged for the September run. The short-term monitoring of PMT gain drifts is done by means of a laser-driven pulsing system [2]. It is not the purpose of the Cs source system.

7 Montecarlo simulation

A Montecarlo simulation of the energy deposited by the Cs^{137} 662 keV photons in the calorimeter was performed. The GEANT based Montecarlo includes a detailed description of the geometry, in particular how the scintillation tiles are interleaved with the iron plates. The thresholds in GEANT to follow the particles of the cascade have been set to the minimum value of 10 keV. The holes in the tiles are situated at 1.5 cm from the edge of the tile. This is of the order of the range of the photons in the iron. Hence, one expects a fraction of the energy to be deposited in the next row of tiles. The estimate of the Montecarlo is that, if the source traverses the upper hole of a tile , 77 % of the energy is deposited in that same row, 22 % in the row of tiles situated on top and 1 % in the row of

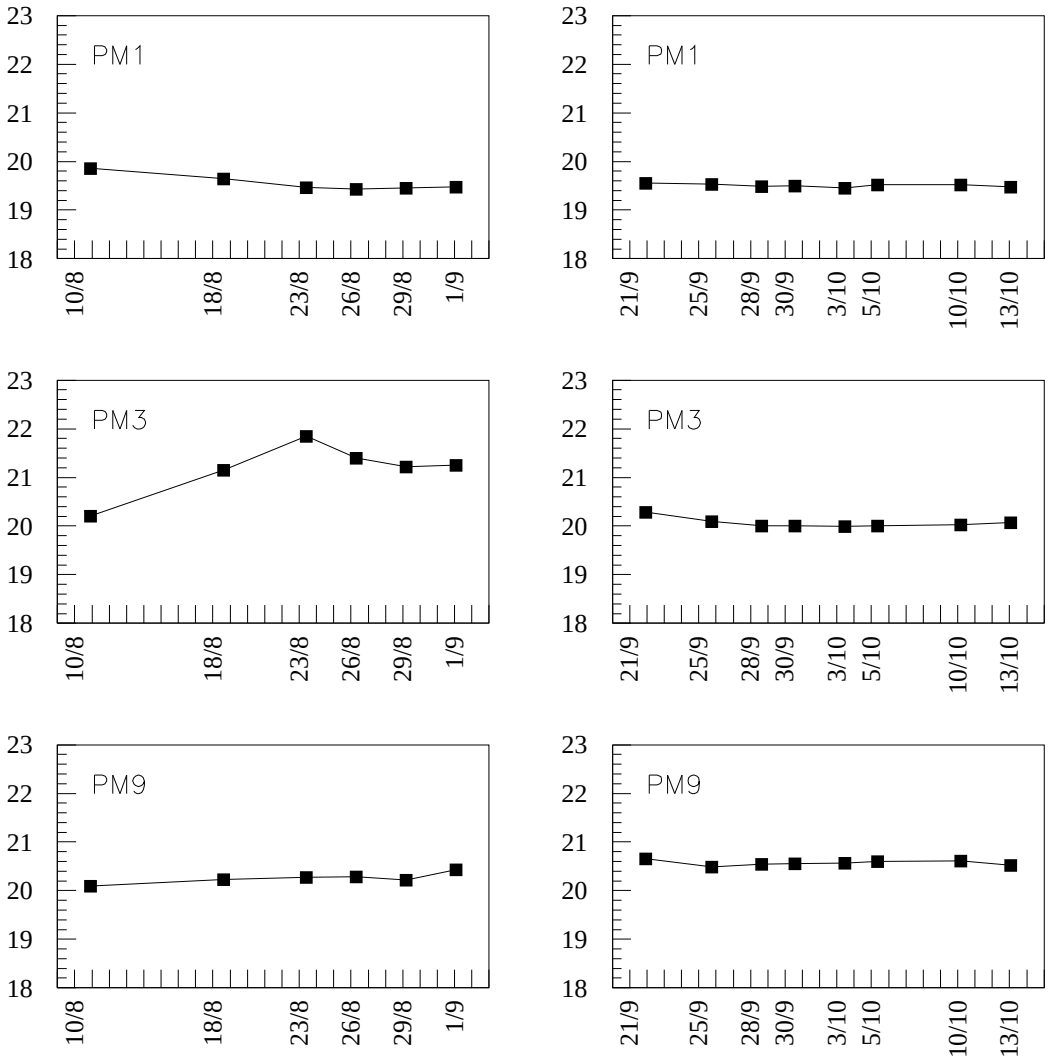

Figure 9: *Gain evolution as a function of time for 3 typical PMTs of the central module. The left column refers to the August run and the right column to the September run. The vertical scale is arbitrary.*

tiles situated below.

More details on how this energy is distributed in the individual tiles of a cell is shown in fig.10. When the source is centered on a scintillator tile, about 50 % of the visible energy is deposited in the tile where the source is situated, and in decreasing amounts in the neighbouring tiles from the same row and the upper row.

The Montecarlo reproduces the peak/valley structure observed experimentally (fig.6). There is more visible energy when the source is centered on a tile than

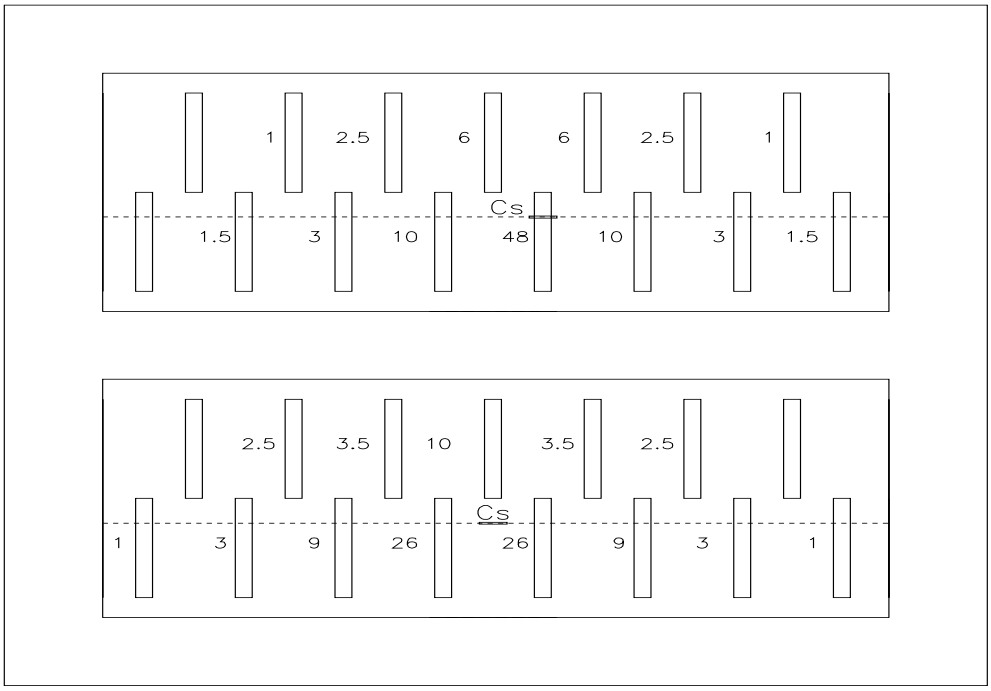

Figure 10: *Fraction of energy in % deposited in the various scintillator tiles of a cell for 2 positions of the source : (top) centered on a tile, (bottom) in between two tiles. The path followed by the source across the cell is represented by a dashed line. The source position is indicated (Cs) along the line.*

when it is centered between tiles. The Montecarlo predicts a ratio of the amplitude of the peak/valley structure to the total height of $14 \pm 1.6\%$ in agreement with the experimental value of $12 \pm 0.3\%$.

8 Tile/fiber fluctuations

The light yield of the tiles forming a cell is not uniform since a cell is comprized of tiles of different widths. In addition, the light yield of tiles of the same size may fluctuate from tile to tile due to manufacturing effects. There may be variations of the light transmission from fiber to fiber as well as in the quality of the tile-fiber coupling. Information about those effects can be extracted from the maxima in the Cs^{137} current spectrum; variations in the light yield of the tile would result in a smaller or larger value of those maxima. Considering that two PMTs read the same tile, both would see the same fluctuation on the tile response, but each of them are connected via different fibers and tile-fiber couplings. Variations in those would affect the corresponding PMT only. Fig.11 shows superimposed the current measured by the right and left PMTs of a cell, divided by their respective gains.

Some of the peaks are well matched, while others present different maximum values for the same tile.

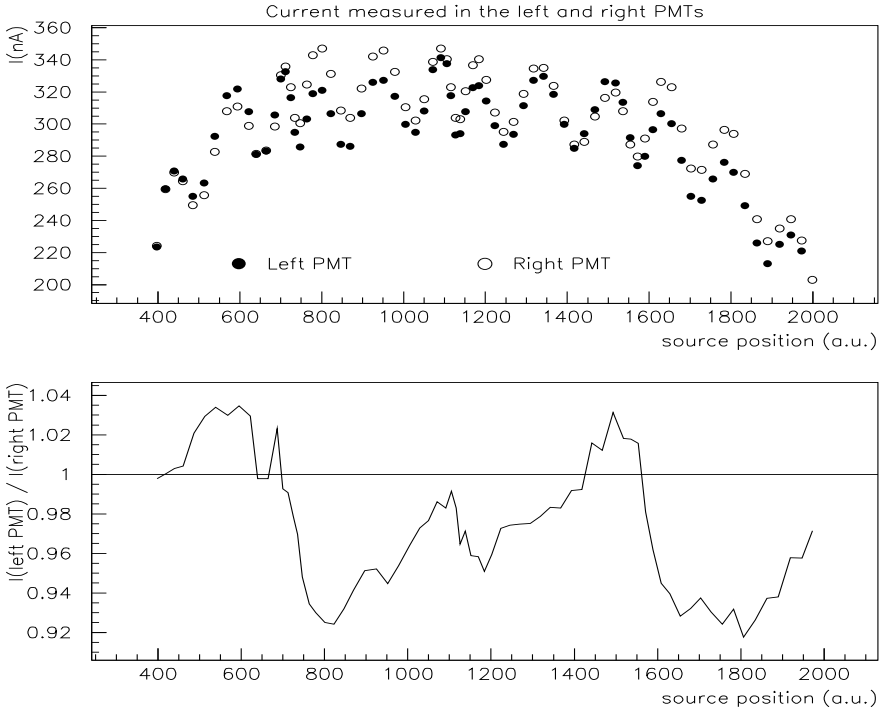

Figure 11: *(top): current spectrum measured by the left and right PMTs of one cell are superimposed; (bottom): their ratio.*

To be able to extract the information on individual tile and fibers, one has to take into account the fact that the energy is distributed over more than one tile. The profile of energy distribution over the neighbouring tiles was extracted from the data : a smooth profile was produced by summing up all measurements and it was fitted to an acceptance pattern of the type shown in fig.10. The result is in good agreement with the Montecarlo pattern. So the data are treated in the following way : for each cell the values of the individual 11 (or 12) maxima are extracted. From these values the response of each tile is calculated by unfolding the contribution of the neighbouring tiles, as described above. To simplify the unfolding an approximation is introduced by neglecting the 22 % of energy deposited in the next row of tiles. The distribution of the individual tile response for the central module is shown if fig.12.

It is a good gaussian distribution (with the exception of about 1 % of tiles in the tail) with sigma = 6.7 %. This width results from both tile-to-tile and fiber-

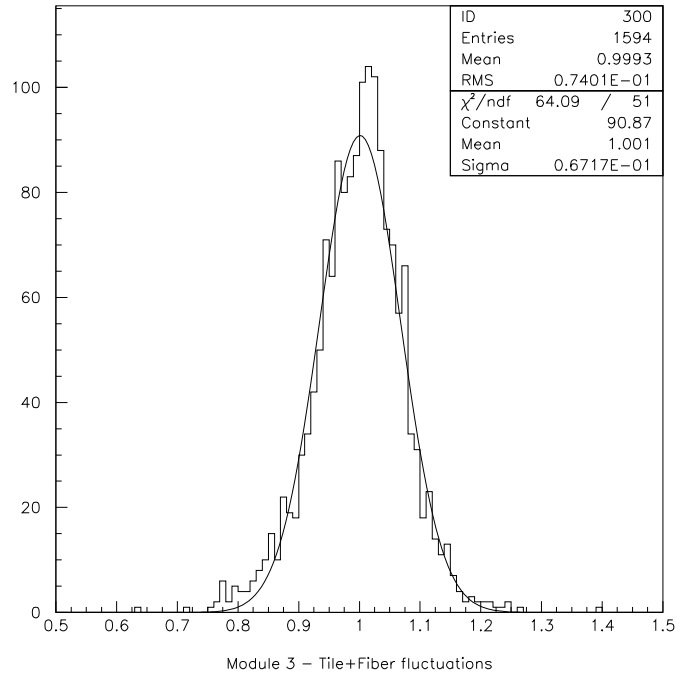

Figure 12: *Dispersion of the values of the unfolded maxima of the current spectra for all readout cells of the central module.*

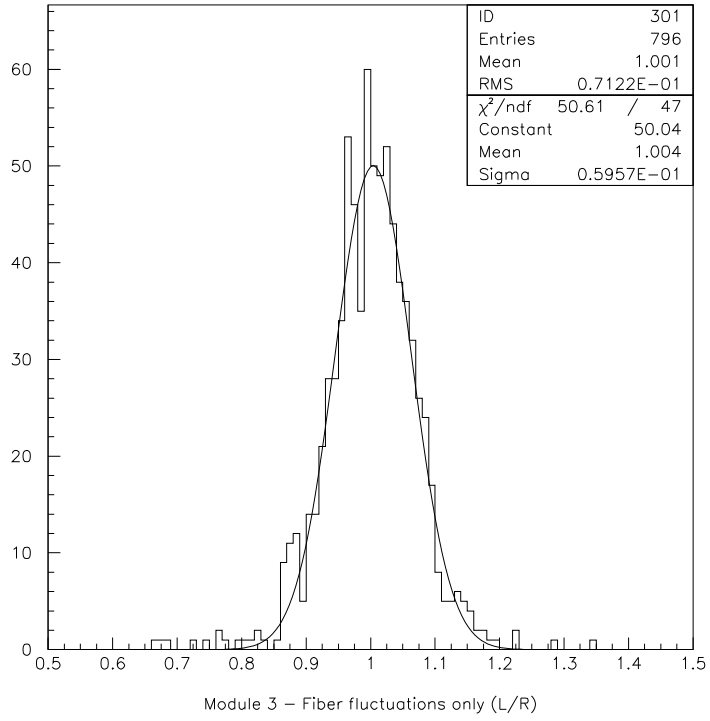

Figure 13: *Ratio of the unfolded maxima of the current spectrum of the left PMT over the right PMT for all cells of the central module.*

to-fiber fluctuations. Looking at the ratio of left and right PMTs measurements, tile fluctuations cancel and only fiber-to-fiber fluctuations will contribute to the width. Fig.13 shows that distribution which has a sigma of 6.0 %. So the contribution of left or right is $\frac{6.0}{\sqrt{2}} = 4.2\%$. Subtracting quadratically the latter value from the total 6.7 %, one extracts a value of 5.2 % for the tile-to-tile fluctuations and the effect of different fiber lengths.

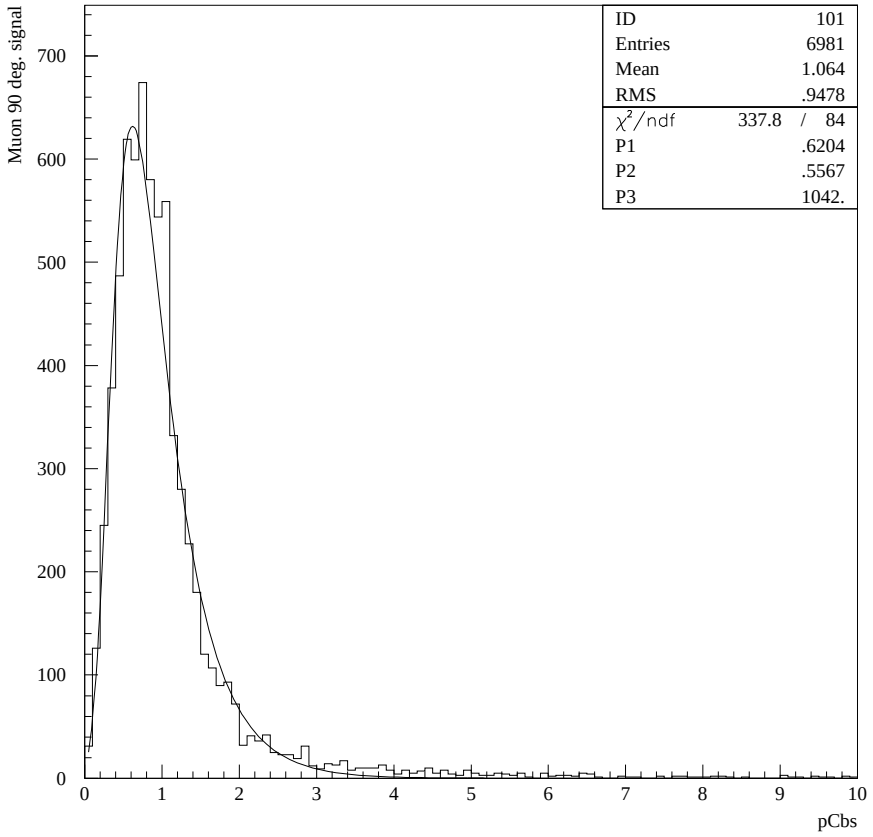

Figure 14: *Typical 200 GeV muon energy spectrum at* 90 deg. *The result of a Moyal fit is also shown.*

9 Correlation of source data with Muon response

The calorimeter was exposed to high energy muons impinging at 90 deg in the geometrical center of the 18 tiles. This provides an alternative technique to intercalibrate the calorimeter cells. In this chapter, we will describe the analysis of the muon data, and then compare source and muon signals. First, source and muon signals will be averaged over the 10 PMTs of a row and the respective

dependence of source and muon signals on the tile number will be discussed. Finally, source and muon signals of individual PMTs will be compared.

9.1 Extraction of the Muon signal

The exposure of the calorimeter to 200 GeV muons was done at the beginning of the August run period. The 18 tiles of the central module and one tile per sampling of the two neighbouring modules were scanned. A typical energy spectrum of the muons is shown in fig.14.

These distributions have been analysed by two different methods. The first one consists in fitting the energy distribution with a Moyal function [3]:

$$F_M(X) = P_3 * exp[-\tfrac{1}{2}exp(-f(X)) + f(X)]$$

where $f(X) = C * \frac{X-P_1}{P_2}$, C is a constant equal to 2.22 and P_1, P_2 and P_3 are the free parameters; respectively the mean, the width and the normalization factor of the distribution. This parametrization, compared to a pure Landau, allows to take into account resolution effects but do not reproduce well the high energy tail due to bremsstrahlung and direct e^+e^- pair creation important at this energy. The fitted peak value provides the gain of the PMT.

The second method is the truncated mean method : the PMT gain is given by the averaged value of the distribution calculated after removing the top 35 % of the events. The two methods gave results that agree to the level of 2.4 % (fig.15 left), indicating that systematic effects in the extraction of the gains are not too large.

Muon signals in the calorimeter are small and the precision could be limited due to the effect of the noise and the resolution of the ADCs. A second set of muon data was recorded one day later, inserting external amplifiers (gain 10) in the electronic chain. The correlation between the two data samples using the Moyal fit is 3 % (fig.15 right) which can be taken as an estimate of the precision of the measurement with muon data. Fluctuations in the gains of the PMTs would also contribute to that width. The correlation between the two muon data sets, using the truncated mean method gives a slightly worse correlation, 4.5%. That could be due to a pion contamination in the muon beam.

9.2 Comparison of Cs and muon signals for the 18 rows of tiles

For each tile size (1-18), the signals given by the corresponding 10 PMTs are averaged to suppress fluctuations due to the precision of individual measurement. The pattern observed across the 18 tiles obtained with the source and muons is shown in fig.16.

If the response of the calorimeter was completely uniform, one would expect for the Cesium a signal of 1 for all tile sizes except the last one of each sampling

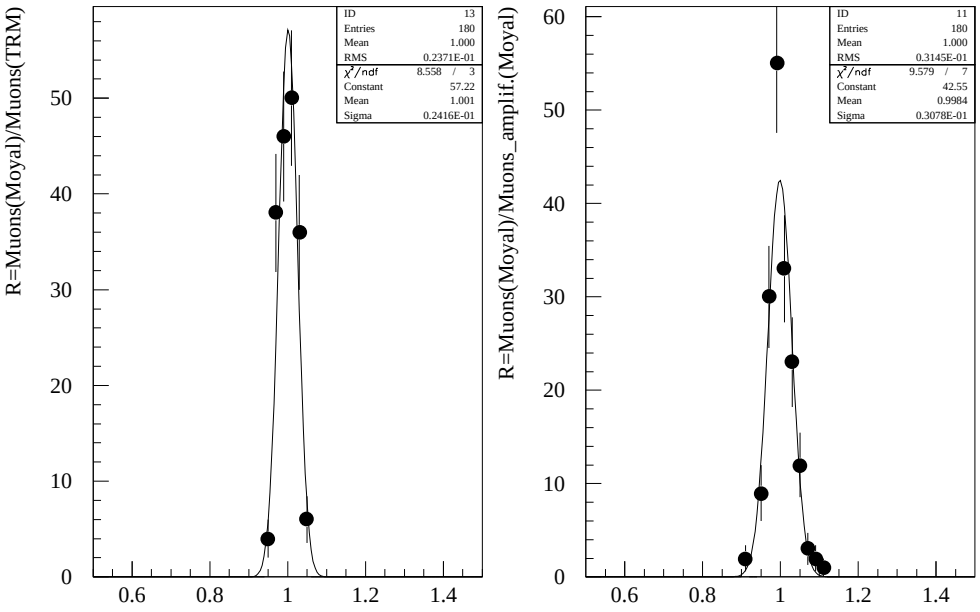

Figure 15: *Analysis of muons at* 90 deg. *The data shown correspond to the 18 tiles of the central module. The distribution on the left shows the comparison between the Moyal and truncated mean methods. The distribution on the right compares the result for the 2 sets of muon data without and with external amplifiers.*

where one expects only a fraction of the energy as explained before. For the muons, the signal should be constant. However in fig.16 a non-uniform pattern is evident, with similar but not equal structure for Cs and muons. This pattern results from the combination of the following effects.

1. The tiles are read by fibers: the absorption length of the fibers is of the order of 2m. The bottom end of the fiber is aluminized and the reflectivity is about 85%. Half of the light collected by the fiber will travel directly to the PMT, while the other half will go to the bottom end, reflect and then travel back to the PMT (fig.17).

   Within a longitudinal sampling, the first, third, etc. tiles are connected to one set of fibers while the second, fourth, etc. tiles are connected to another set. The fibers of the latter set are 10 cm shorter than the fibers of the former set (fig.17). So within a given sampling, depending in which tile the energy is deposited, the efficiency of light collection in the fibers will be different.

2. The tiles become progressively larger as one goes from the inner to the outer detector radius. The distance from the center of the tile to the fiber

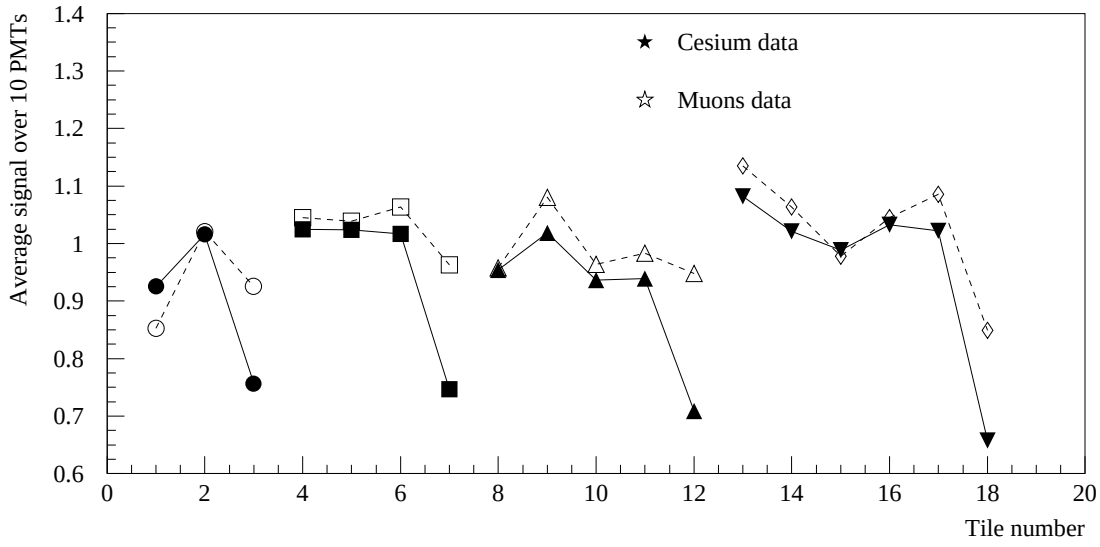

Figure 16: *Comparison between the Cs and muon data for the central module. Each point is the average of the signals from the 10 PMTs corresponding to that tile. The muon data are normalized to their mean value, while the Cs data are normalized to their mean value after removing the last point of each sampling (since in that case only 78 % of the energy is deposited in the tile).*

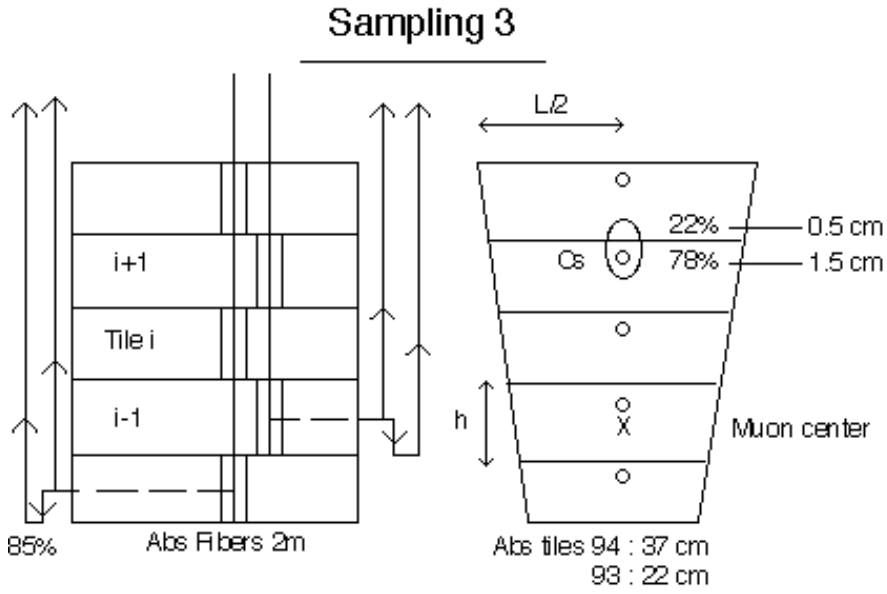

Figure 17: *Schematic representation of the third sampling containing five rows of tiles. On the left, the connections of tile to fiber are illustrated as well as the path followed by the light inside the fibers. On the right, the varying tile width is represented together with the location of the energy deposited by Cs and muons.*

increases by about 5mm going from one tile size to the next, hence more light is absorbed in the tile.

3. The transmission of light from tile and fiber has some dependence on whether the light was generated in the center of a tile (as for muons) or at 1.5 cm from the edge (as for Cs γ's).

A simple model was developed to take those effects into account. In case of muons, the energy is deposited in the geometrical center of the tile. The absorption of light in a tile is calculated assuming 37cm absorption length [4]. The length of fiber corresponding to each tile is calculated and the light absorption is estimated using a 2 m absorption length and 85 % reflectivity. In the case of Cs, it is assumed that 78% of the energy is deposited in a point at the center of the tile in width but at 1.5cm from the upper edge, while 22% is deposited in the next tile at 0.5cm from the lower edge. Fig.18 shows the result of the model compared to the Cs data.

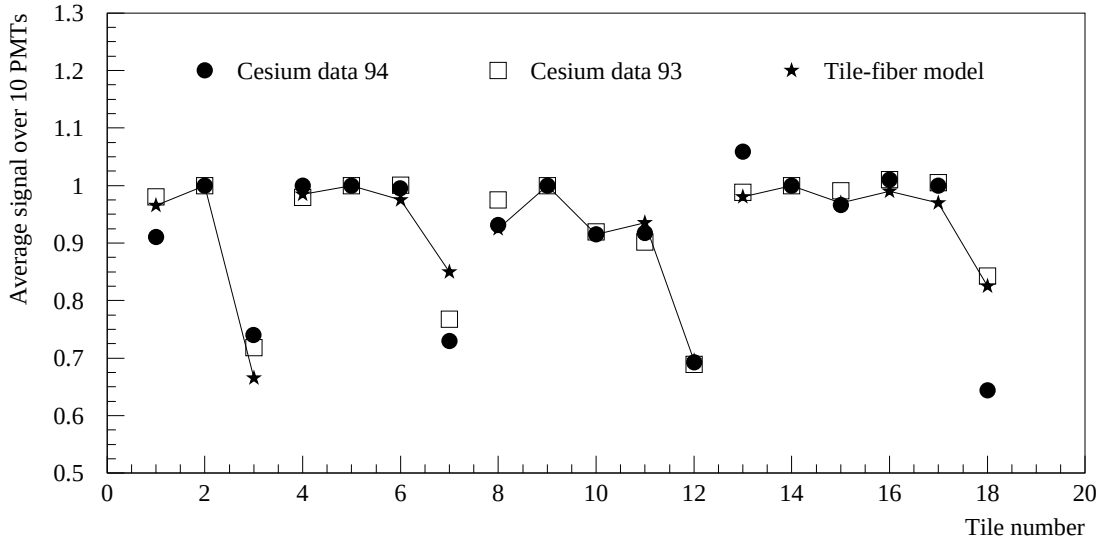

Figure 18: *Average Cs signal over 10 PMTs for the 18 holes of the central module. '94 and '93 test beam data are compared to a simple model taking into account fiber length and tile width variations.*

Clearly the pattern is in first approximation well reproduced indicating that those effects are indeed the origin of the structure. On the same figure are shown the data of the '93 test beam for another module, similar in construction except for the absorption length of the tiles (22cm instead of 37cm). The pattern observed is similar to the '94 pattern except for a few tiles. The model predicts that the profile should not change significantly for a different absorption length as long as the absorption length is the same for all tile sizes. In 94, some tiles

of sampling 1 and sampling 4 (like tile size 1 and tile size 18) were produced with a different material and had shorter absorption length. Hence they produce relatively less light, with respect to other tiles in the same sampling, than in '93.

When trying to correlate Cesium with Muons, one has to take into account the fact that the Cesium source deposits energy across 2 tiles and hence form the ratio Cs over Cs reconstructed from the muon signal, i.e.

$$Cs_i = 0.78 * \mu_i + 0.22 * \mu_{i+1}$$

where i is the tile number, within a given sampling (fig.19).

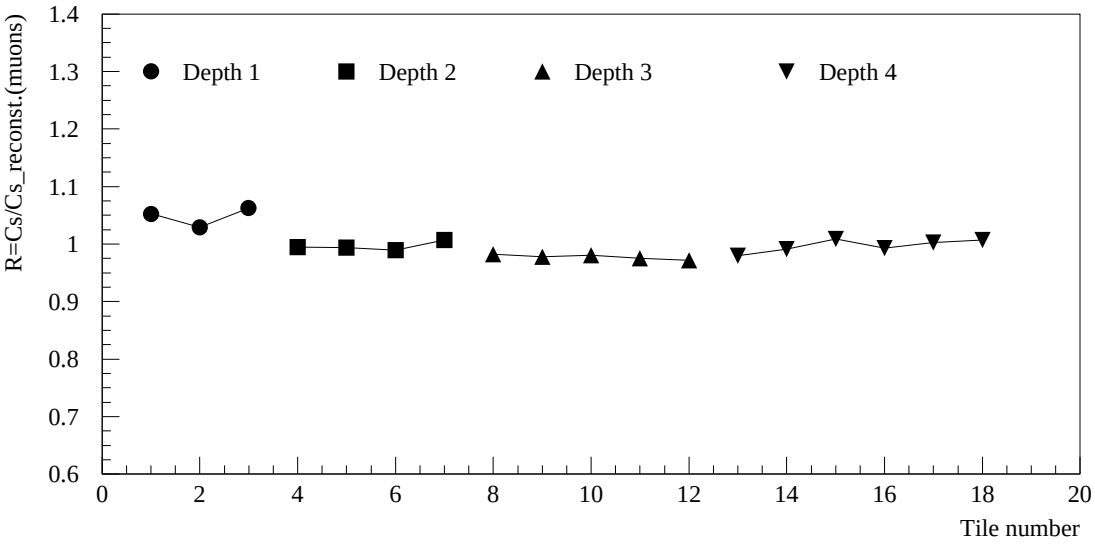

Figure 19: *Ratio of Cs over Cs reconstructed using muon data. The signal is averaged over the 10 PMTs corresponding to a given tile. Cs reconstructed = 0.78*muon(i) + 0.22*muon(i+1).*

In this ratio, the effects responsible of the pattern cancel to the first order but not completely. Sampling 1 and 4 suffer from the problem of different absorption length of some tiles, so sampling 2 and 3 should be taken as the most representative of the correlation source-muons. The data show for those two samplings a dispersion of 1%. For all tiles, the dispersion is 2%.

9.3 Source-muon signal correlation within a row of tiles

For a given tile size, the ratio Cs signal over muon signal taking into account the tile mixing factor (see section 9.2) is plotted as a function of the PMT number. Fig.20 presents the result for the 4 samplings of the central module. Each individual distribution shows a large dispersion.

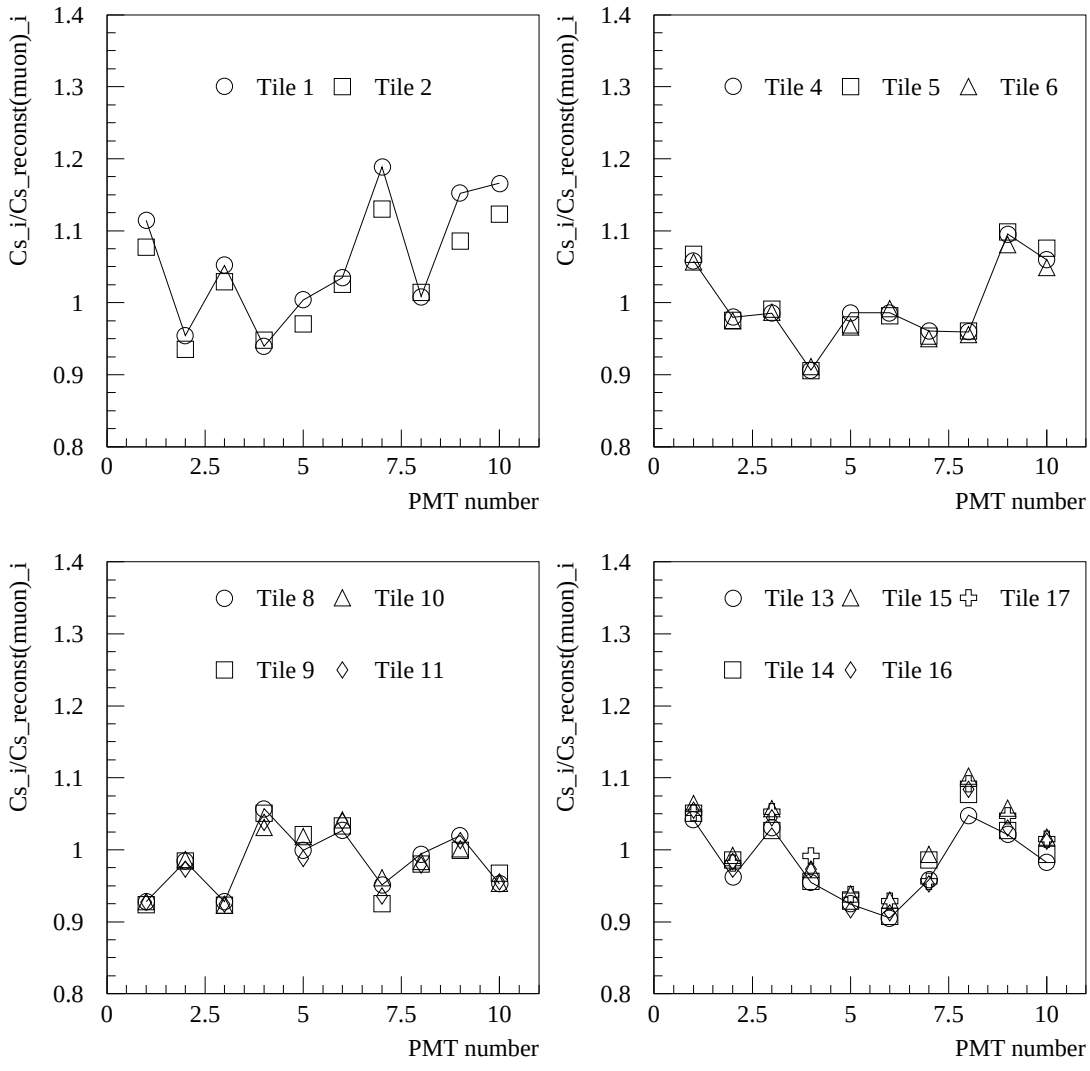

Figure 20: *Ratio Cs over Cs reconstructed using muon data for individual PMTs (see text). The 4 plots correspond to the 4 samplings. For each sampling, the result for each tile size is superimposed.*

The dispersion vary from 8% in sampling 1 to 5-6% in the other samplings. However, a clear systematic effect appears when comparing the 10 PMTs of a given tile size to another one of the same sampling. The pattern clearly repeats from one tile to another in the same sampling.

Variations of gains of the PMTs in the interval of time that separates the Cs and the muon data could produce an effect of that type, but their magnitude and sign are not correlated with the observed pattern. Such a behaviour could result as well from some miscalibration in the Cs or in the muon chain. The problem is being investigated.

9.4 Overall source/muon signal correlation

After correcting for the tile mixing factor, the ratios of the Cs to the muon signals are shown in Fig.21. The distribution has a dispersion of about 6%, which arises -as shown in the previous discussion- by a systematic dispersion within each row of tiles.

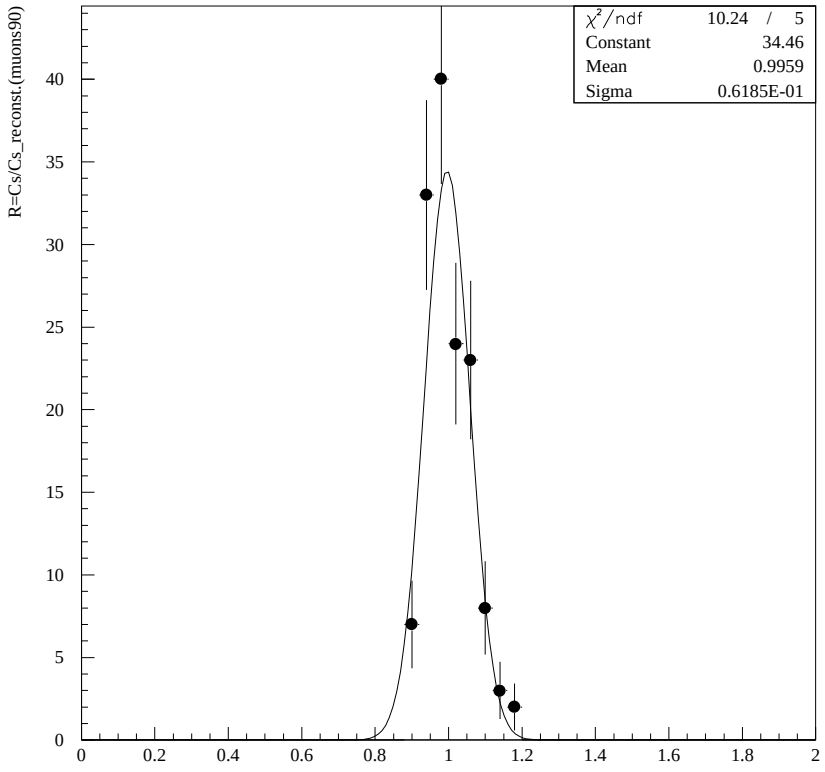

Figure 21: *Ratio of Cs to reconstructed Cs with muon data for individual PMT*

10 Conclusion

A system to intercalibrate the Tilecal '94 prototype, with entirely new hardware, readout and data acquisition, was built and operated this year. Using this system, the 200 prototype readout cells were intercalibrated; the system allows to measure the response of all 18 tiles in a module in two hours. Several such scans were performed during the August and September/October test beam runs.

The calibration constants obtained with this system are precise to better than 1%; however, over two weeks, variations of several percent in the response of about one third of the PMTs of the central module were observed. These variations appear to be associated to the PMTs themselves.

Using the large data base accumulated this year, the uniformity of the calorimeter has been studied in detail. It is possible to separate the response fluctuations due to differences in fiber coupling and those due (mostly) to tile response variations; the former have varied 4.2%, the latter 5.2%.

An extensive study of the correlation of the response of the calorimeter cells to muons at 90 deg to the tiles and to the Cs source has been performed. The conclusion is that the ratio of these two signals is uniform at the 2% level across all 18 tile sizes; however sytematic cell-to-cell effects appear at the 6% level. These are clearly associated with either the muon or the source readout.

More work is in progress, to further reduce the scanning time and to eliminate the remaining dispersion in the muon/source response ratio. The current performance level is consistent with intercalibration needs within ATLAS.

References

[1] F. Ariztizabal *et al.*, Nucl. Instr. and Meth. **A349** (1994) 384.

[2] ATLAS Collaboration, CERN/LHCC **93-51** (1993).

[3] E. Moyal, Phil. Mag. **46** (1955) 263.

[4] A. Amorim *et al.*, Measurements of Tilecal scintillators, Tilecal Internal Note.